CHAPTER 5 PHYSIOMECHANICAL, FLOWABILITY AND ANTIBACTERIAL CHARACTERIZATION OF SILVER-DOPED EGGSHELL-DERIVED HYDROXYAPATITE FOR BIOMEDICAL APPLICATIONS

In this chapter, the results and discussions on silver-doped eggshell-derived HAp powder which are synthesized with varying weight percentages (0.0, 0.1, 0.2 and 0.5 wt %) of silver nitrate ($AgNO_3$) in HAp were done. The compacted and sintered samples were used to investigate the physiomechanical behavior through the determination of relative density, porosity %, compressive strength, and Vickers microhardness tests, etc. The flowability and antibacterial properties were determined. Later, the Inductively Coupled Plasma Mass Spectroscopy (ICPMS), X-ray diffraction Technique (XRD), Fourier Transform Infrared spectroscopy (FTIR), Scanning Electron Microscopy (SEM), and Energy Dispersive Spectroscopy (EDS) verified the morphology, chemical composition, bonding strength, crystallite size, particle size, lattice strain and phase purity. Six different bacteria strains, i.e., *S. epidermidis, S. aureus, B. subtilis, E. Coli DH5α, P. aeruginosa* and *E. Coli*, employed for antibacterial characterization confirm the antibacterial nature of silver-doped HAp. Also, the wettability and thermal characterizations were performed to establish the hydrothermal stability of synthesized samples.

5.1 Results and discussion

5.1.1 Flowability Analysis

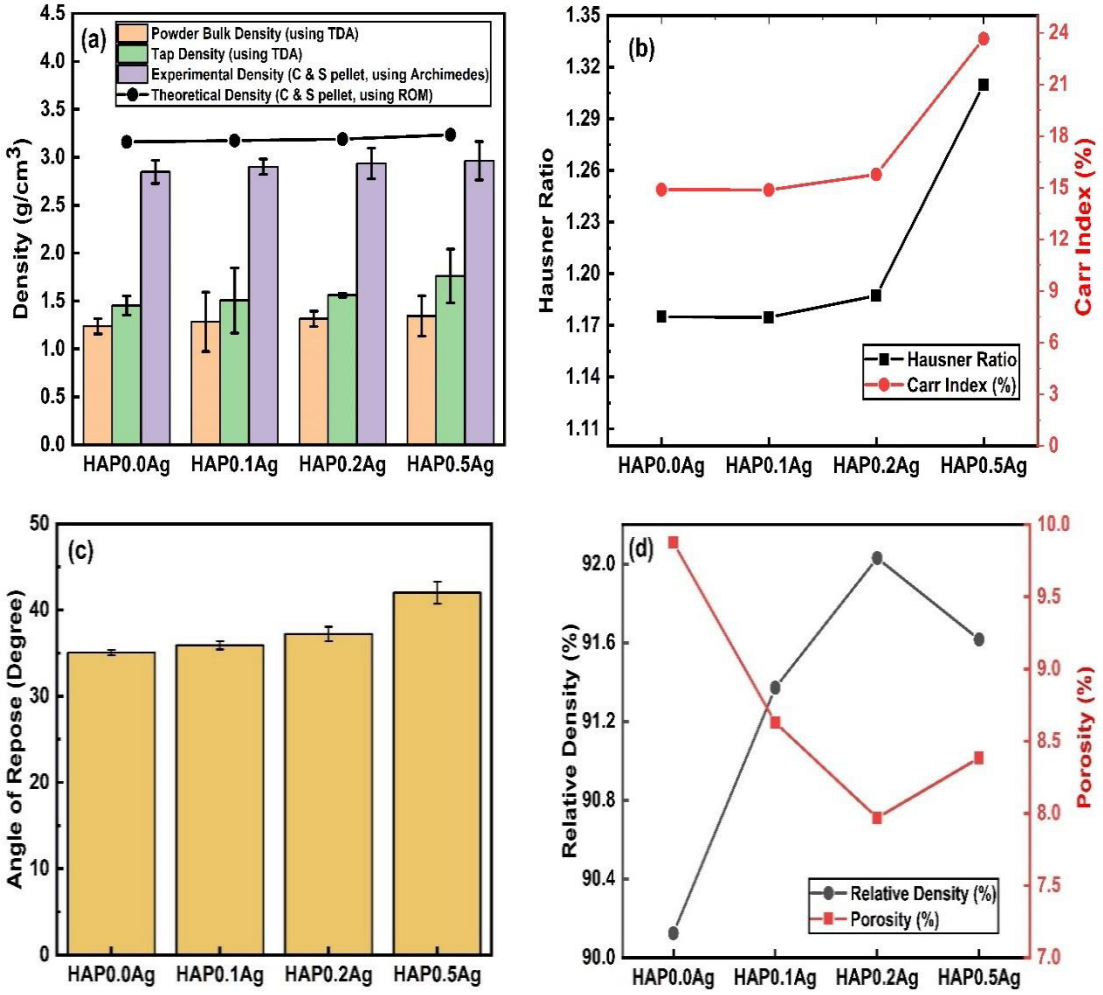

Fig. 5.1 (a) Density **(b)** Hausner Ratio and Carr's Index, **(c)** Angle of repose and **(d)** Relative density and porosity percentage of HAP0.0Ag, HAP0.1Ag, HAP0.2Ag and HAP0.5Ag samples.

The bulk density, tap density, Hausner ratio, Carr's index, angle of repose and the flow characteristics of silver-doped HAp were evaluated and tabulated in **Table 5.1**. The output reveals that HAP0.0Ag and HAP0.1Ag samples represents "GOOD" flow characteristics with an angle of repose less than 36^0, whereas HAP0.2Ag and HAP0.5Ag show "fair" and "travelable" flow respectively. As observed, the density of the powdered and the sintered samples increases with an increase in the doping percentage of silver ions in the HAP. **Fig. 5.1 (a)** illustrates that the difference between

the average tap density and true density for HAP0.0Ag, HAP0.1Ag, HAP0.2Ag and HAP0.5Ag samples are 48.96 %, 48.07 %, 46.41 % and 40.38 %, respectively. The difference is due to a reduction in void volume fraction during compact preparation. As per Campbell [172], the porosity, hydrophilicity and hydrophobicity depend on the sample's bulk/ tap density, and the porosity decreases with an increase in density. The bulk density and the tap density are responsible for calculating the Hausner ratio and Carr's index (shown in **Fig. 5.1 (b)**) which embodies the flowability of the powdered sample. Kaleem et al. [143] reported the justification of good flow characteristics in the additive manufacturing process using the Hausner ratio and Carr's Index analysis on powdered precursors. The series assessment is made by using the standard chart shown in Chapter 3, table 3.1. It is worth noticing that, the compressibility index or Carr's Index determines the compressibility, adhesiveness, maximum packing efficiency and other granular quantitative matrices of the powdered samples as testified by Amidon et al. [173]. The angle of repose shown in **Fig. 5.1 (c)** determined experimentally using ISO 8398: 1989 of the free-flowing powder samples HAP0.0Ag, HAP0.1Ag, HAP0.2Ag and HAP0.5Ag are 35.06 ^{o} ± 0.32^{o}, 35.69^{o} ± 0.47^{o}, 37.22^{o} ± 0.83^{o} and 42^{o} ± 0.28^{o}, respectively. It is an imperative parameter to define the flow characteristic of the powdered sample used for bio coatings [151]. Flowability promotes the development of biofilms on implants which reduces periprosthetic infection [174]. Silver doping in HAp improves crystallinity and can be the main reason for the increase in the angle of repose with increasing doping percentage. As investigated by Kudo et al. [151], particle size and shape are directly related to flow characteristics. The smaller the particle size, the larger the inter-particle friction that reduces its flowability; similarly, the particle's irregular shape provides hindrance and affects its macro movement. The flow property reveals "GOOD" flow characteristics

for HAP0.0Ag, HAP0.1Ag, “FAIR” for HAP0.2Ag and “TRAVELABLE” for HAP0.5Ag powdered sample as listed in **Table 5.1.** The results concludes that the silver-doped HAp has acceptable flowability and can be used for coating applications for implants.

The relative density percentage (**Fig. 5.1 (d)**) for HAP0.0Ag, HAP0.1Ag, HAP0.2Ag and HAP0.5Ag sintered samples are 90.1247 %, 91.3671 %, 92.7689 % and 91.2975 %, respectively, and porosity percentages are 9.8753 %, 8.6429 %, 7.2310 % and 8.7024 %, respectively. Results obtained reveal that the maximum doping permissible in HAp can be restricted to 0.2 wt% as it has maximum relative density and minimum porosity for the same compaction pressure and sintering temperature. Therefore, HAP0.2Ag with comparatively highest relative density percentage will have minimum compressibility and maximum surface hardness. The result is also justified for maximum compressive strength and young modulus of the sintered samples.

Table 5.1. Bulk density, Tap Density, average angle of repose, Hauser’s ratio, Carr's index and flow property of HAP0.0Ag, HAP0.1Ag, HAP0.2Ag and HAP0.5Ag powder samples.

Sample	Bulk Density (Powder)	Tap Density (Powder)	Angle of Repose	Hausner Ratio	Carr's Index (%)	Flow Property
HAP0.0Ag	1.24 ± 0.08	1.45 ± 0.10	35.06 ± 0.32	1.175	14.89	GOOD
HAP0.1Ag	1.28 ± 0.31	1.51 ± 0.34	35.90 ± 0.47	1.175	14.87	GOOD
HAP0.2Ag	1.31 ± 0.08	1.56 ± 0.02	37.22 ± 0.83	1.187	15.77	FAIR
HAP0.5Ag	1.34 ± 0.55	1.76 ± 0.28	42.00 ± 1.28	1.309	23.65	TRAVELABLE

5.1.2 Mechanical Characterization

5.1.2.1 Compression Test

As illustrated in **Fig 5.2 (a-b)**, the compression test results of the eggshell-derived and sintered HAp samples with varying silver doping concentrations i.e. HAP0.0Ag, HAP0.1Ag, HAP0.2Ag and HAP0.5Ag. Compression properties of cylindrical

samples (approximately 10mm dia and 20mm height) prepared as per ISO 17162: 2014 (for advance ceramics). **Figure 5.2 (a)** shows the stress-strain relationship obtained through the compression test. As observed, **Fig. 5.2 (b)** shows the maximum compression strength (MCS) 146.40 MPa of the HAP0.2Ag sintered sample. An increase of 5.52 % is observed between pure and 0.2 % silver-doped HAp which shows the improved adhesion and bonding strength of silver doping in HAp till 0.2 %. The sintered HAp samples shows compressive strength between 130 MPa to 150 MPa and young modulus between 5-7 GPa that correlates with the MCS range as reported by Martin & Brown [175]. The high yield stress and low young modulus are desired for biomedical applications to avoid the stress shielding effect. The strength of the human cortical bone is approximately between 90-209 MPa [176]. Barabashko et al. [177] in 2019 reported that the variation in MCS can be due to the inhomogeneous distribution of silver doping in bioceramic HAP. A slight decrease in the MCS value in HAP0.5Ag limits the doping percentage in HAp. The **Fig. 5.3 (a-d)** shows the internal SEM images of the sintered samples after the compression test failure. The micro-cracks, internal pores and powder dispersion illustrate the brittle failure of samples. Crushing failure of HAP0.2Ag is observed in **Fig. 5.3 (c)**. Undoped HAp fails due to a sudden crack run during high load compression. SEM micrograph shown in the **Fig. 5.3 (d)** interprets the high dispersion of Ag in HAp at 0.5 M% concentration and thus can be the reason for a decrease in compressive strength. Young modulus increased by 18.32 % between undoped and 0.1 % molar concentration doped HAp sample. Maximum young modulus i.e., 6218.34 MPa is attained by the HAP0.2Ag sample which is 32.92 % higher than the undoped HAP. Orlovskii reported compressive strength between 88-164 MPa and young Modulus 3.9- 11.7 GPa for the cortical bone [178]. Therefore,

increased compressive strength with antibacterial properties can be seen in HAP0.2Ag powder-based samples.

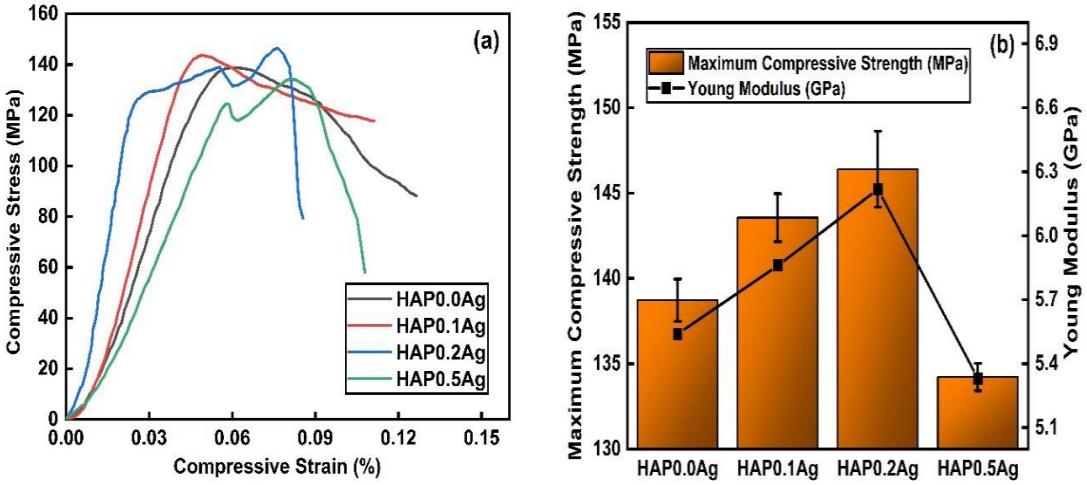

Fig. 5.2. Compression Test (a) Stress-Strain curve (b) Maximum Compressive Strength and Young Modulus for silver doped HAp samples.

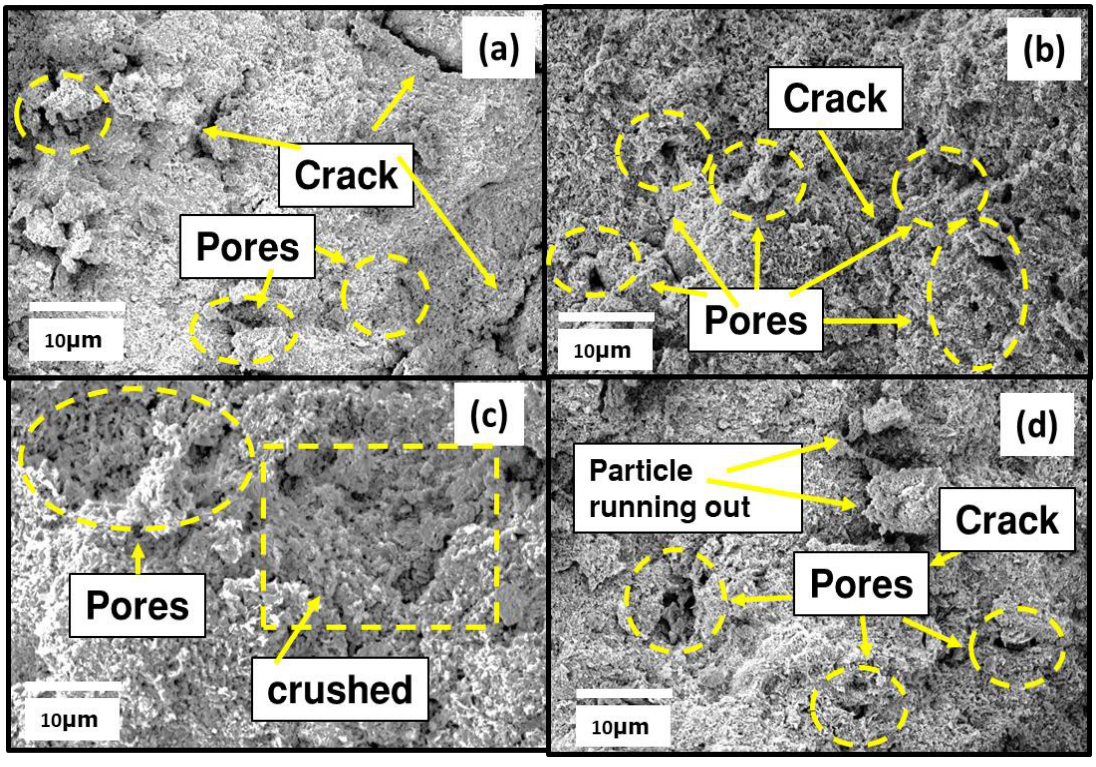

Fig. 5.3. Benchtop SEM morphology of the samples after compression test **(a)** HAP0.0Ag **(b)** HAP0.1Ag, **(c)** HAP0.2Ag, and **(d)** HAp 0.5Ag.

5.1.2.2 Vickers microhardness

Vicker's microhardness value of the HAP0.0Ag, HAP0.1Ag, HAP0.2Ag and HAP0.5Ag sintered samples shown in **Fig. 5.4** are 25.63 ± 0.568 HV, 29.37 ± 0.663 HV, 31.70 ± 0.989 HV and 30.03 ± 0.440 HV, respectively. The 23.68 % increase in hardness is observed between undoped and 0.2 % molar concentration based HAP. The increase in hardness value can be due to the increase in true density and adhesion strength of the silver doped HAp upto HAP0.2Ag. The decrease in hardness for HAP0.5Ag also reflects the decrease in compressive strength and young modulus. Hariani & Salni [179] also reported Vickers's hardness of 20.6 ± 0.62 HV derived from fish bone sintered at 1100 ^{0}C for 2 hours. Similarly, Wu et al. reported Vickers's hardness of 33.30 HV for cortical bone [171], which resembles almost 95.2 % similarity to the HAP0.2Ag.

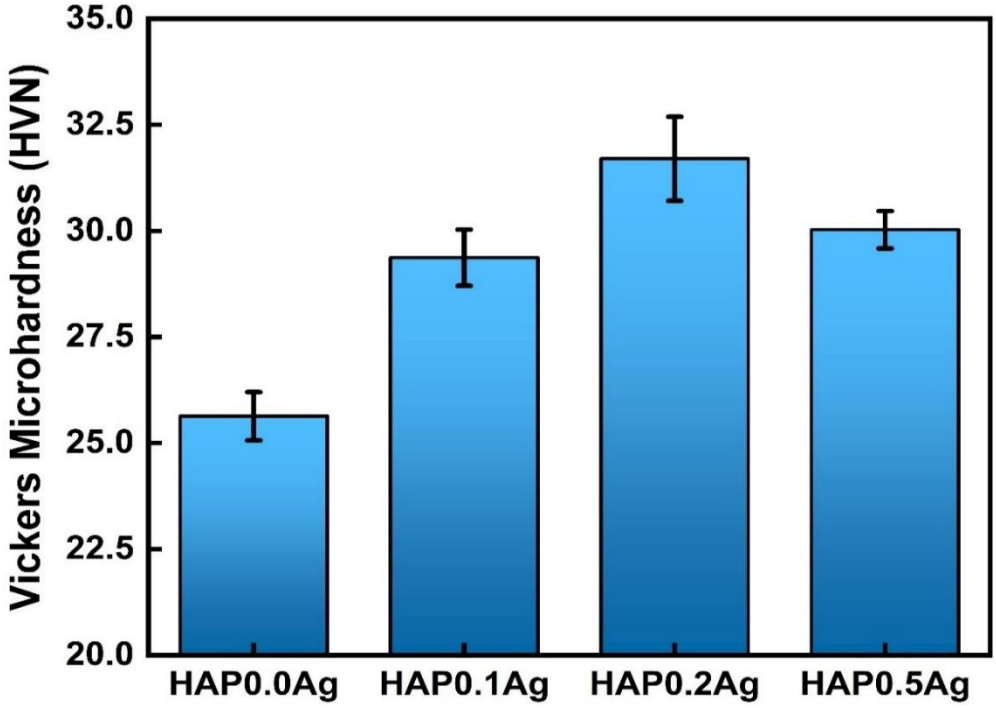

Fig. 5.4. Vickers microhardness of eggshell-derived silver-doped hydroxyapatite samples.

5.1.3 Morphology Analysis

SEM images of HAP0.0Ag, HAP0.1Ag, HAP0.2Ag and HAP0.5Ag are represented in **Fig. 5.5 (a-d)**. The morphology of the synthesized samples shows clear dispersion of silver ions on the surface. As observed, all the surfaces of the as prepared bioceramics exhibit porous microstructure. Yuan et al. [180] reported that the porous powder used for biomedical coating provides good adhesion to natural bone. An increase in the dispersion of dopant is observed at HAP0.5Ag, whereas fine microparticles are observed till 0.2 % molar concentration of silver doping. The flower-like morphology [153] of HAP0.0Ag (as seen in **Fig. 5.5 (a)**) converts to cylindrical and irregular shapes in HAP0.1Ag and HAP0.2Ag, respectively. Irregular and crystalline morphology of silver-doped HAp is also reported by Bee et al. [181]. The morphology change can be due to the dispersion of Ag^{+} ions during doping, redefining the final powder sample's particle size and morphology. Clear dispersion of $AgNO_3$ is visible in the HAP0.5Ag micrograph (**Fig. 5.5 (d)**) and thus the morphology predicts to restrict the doping molar concentration to 0.5 percent.

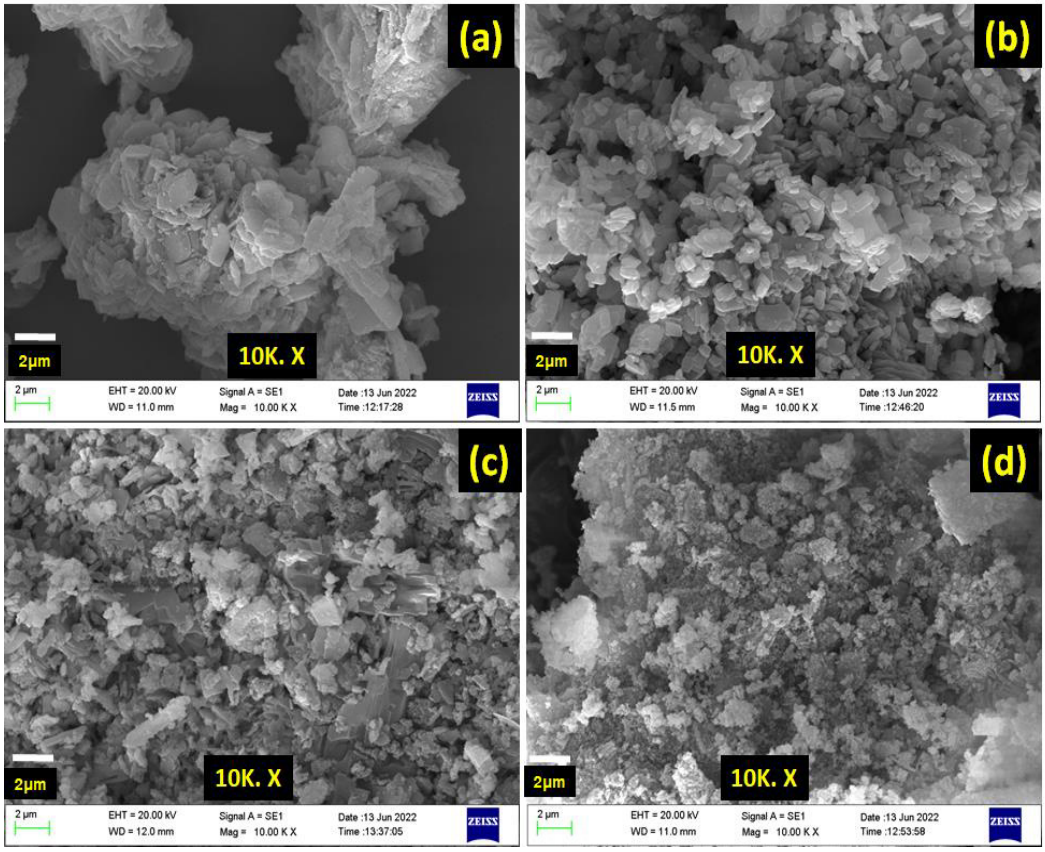

Fig. 5.5. Scanning Electron Micrographs of **(a)** HAP0.0Ag, **(b)** HAP0.1Ag, **(c)** HAP0.2Ag and **(d)** HAP0.5Ag powder at 10K magnification.

5.1.3.1 Particle Size Analysis

The average particle size of HAP0.0Ag, HAP0.1Ag, HAP0.2Ag and HAP0.5Ag is shown in **Fig. 5.6 (a-d)**. Twenty random readings per sample obtained from the SEM images predict that the synthesized sample's particle size ranges from 5 µm to 40 µm. Kudo et al. [151] correlated the relation between particle size and flowability of the powdered samples. The average particle size of HAP0.0Ag, HAP0.1Ag, HAP0.2Ag and HAP0.5Ag are 22.2737 ± 7.092 µm, 21.9525 ± 6.435 µm, 18.8612 ± 6.338 µm and 17.3025 ± 6.21 µm, respectively. A decrease in particle size with an increase in silver doping is observed during the random measurement with a minimum of 8.85 µm and a maximum of 37.35 µm in HAP0.2Ag. The trend arises due to the agitation of doped Ag^{+} ions during chemical synthesis. The normal distribution curve on the histogram chart concludes that the overall average particle size of synthesized HAp

will be approximately 20.02 µm obtained using multistage calcination and chemical dispersion method. Plasma spray coating of HAp with particle size between 10- 90 µm provides good adhesion strength in implant coating and biomedical applications [182]. Also, micro-sized particles show good osteointegration behavior as reported by Albayrak et al. [183] while coating HAp on a titanium substrate with an electrophoretic deposition method.

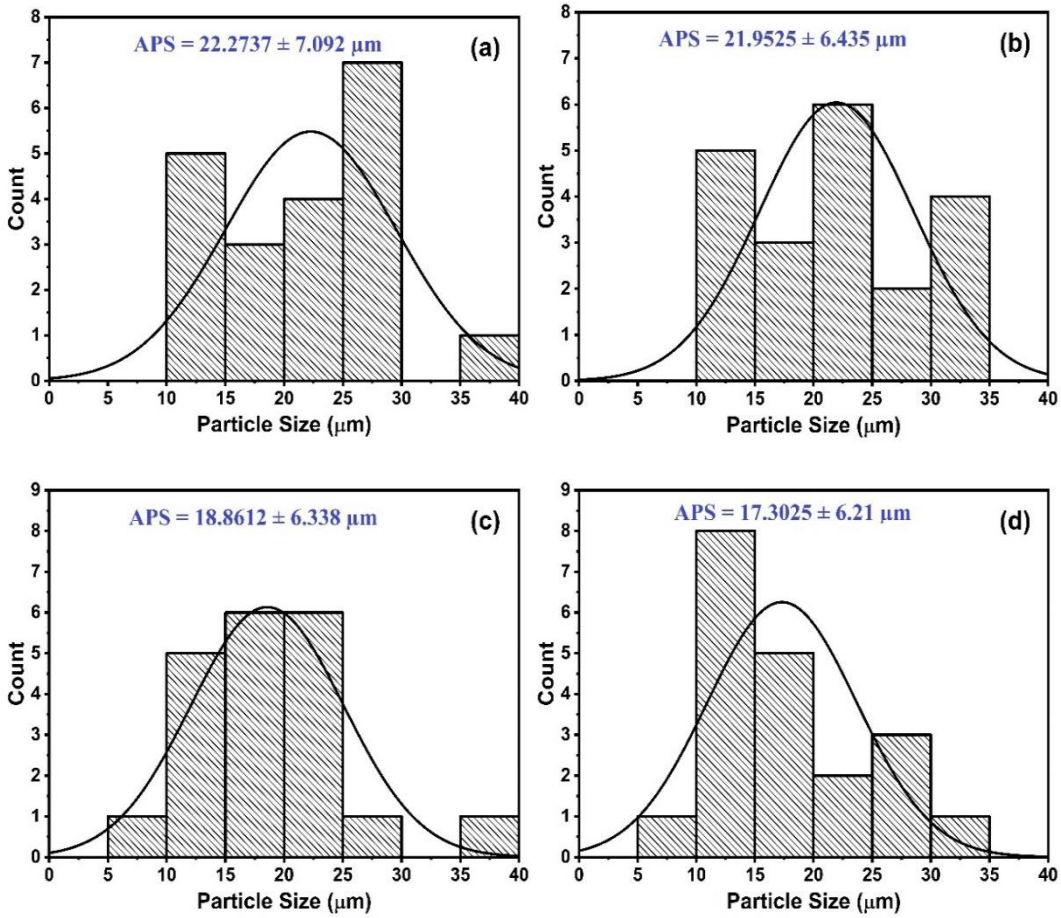

Fig. 5.6. Particle size analysis using Histogram graph of **(a)** HAP0.0Ag, **(b)** HAP0.1Ag, **(c)** HAP0.2Ag and **(d)** HAP0.5Ag samples.

5.1.3.2 EDS analysis

The EDS outputs of the prepared samples are shown in **Fig. 5.7 (a-d**. The graph undoubtedly highlights the presence of calcium, phosphorous, oxygen and silver elements in varying percentages in HAP0.0Ag, HAP0.1Ag, HAP0.2Ag and

HAP0.5Ag. **Fig. 5.7 (a)** is undoped HAp, and hence no trace of silver ions is visible in the spectras whereas a small trace of Ag^{+} is visible in all other compositions (**Fig. 5.7 (b-d)**). Elements present in the HAp were identified, and the (Ca+Ag)/ P ratio shows an acceptable range as per ISO 13779-3 2008 (en) standard used for crystallinity and phase purity of biocompatible hydroxyapatite. The (Ca+Ag)/ P ratio for HAP0.0Ag, HAP0.1Ag, HAP0.2Ag and HAP0.5Ag are 1.668, 1.6607, 1.6569 and 1.661, respectively. The range is 99.8 % close to the stoichiometric ratio of natural bone composition and permits the use of eggshell-derived HAp in biomedical applications.

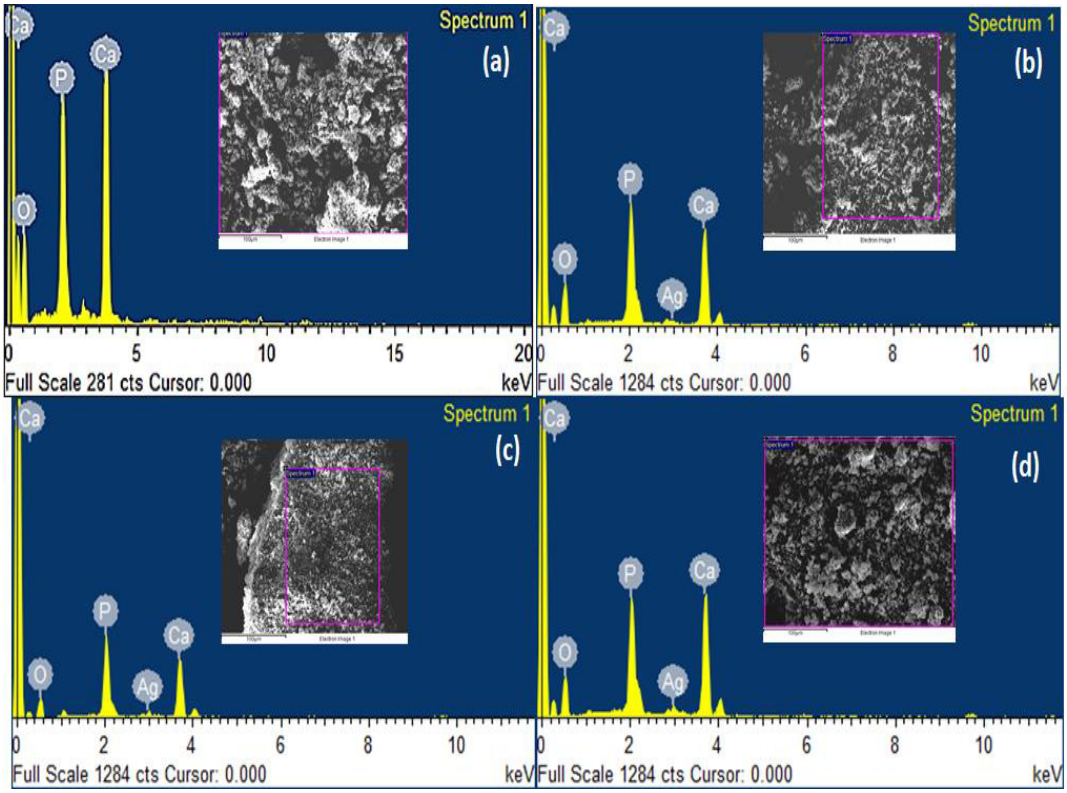

Fig. 5.7. SEM- Energy Dispersive Micrographs of **(a)** HAP0.0Ag, **(b)** HAP0.1Ag, **(c)** HAP0.2Ag and **(d)** HAP0.5Ag.

5.1.4 FTIR Analysis

FTIR analysis shown in **Fig. 5.8** depicts the presence of functional groups in the synthesized Ag-doped HAp samples. The initial bands at 607.23 cm-1 and 657.01 cm-

^{1} are attributed to the O-P-O bending mode [184]. Multiple deep bands between 1050 cm^{-1}- 850 cm^{-1} region confirm the formation of the $PO4^{3-}$ functional group with parallel P-O vibrations [185]. The bands at 1065.84 cm^{-1}, 987.55 cm^{-1} and 861.61 cm^{-1} were noticed as large intensity v_3 asymmetric stretching mode of O-P-O. The results obtained are similar to spectral characterizations obtained by Kumar et al. [186] and Chappard et al. [187] during the synthesis of HAp from natural bone and subchondral bone respectively. Peaks at 1631.09 cm^{-1} and 3329.47 cm^{-1} are attributed to the v_2 bending mode of the O-H functional group. A small molar concentration of Ag^{+} ion doesn't much affect the stretching and bonding strength of the HAPs functional group but a clear rising transmittance peak at 1384.33cm^{-1} reflects the presence of silver-based bonding in the final formation. FTIR spectra peaks between 1065 - 1100 cm^{-1} due to silver doping are reported by Iconaru et al. [188]. A large number of peaks in the fingerprint region (1500cm^{-1} - 450cm^{-1}) verifies the conjugate formation of crystalline bioceramics. The broad band between wave number 2750cm^{-1} - 2950cm^{-1} in all the samples shows the symmetric stretching of hydrated silver-doped HAp samples. All the available peaks are corelated with the literature as listed in **Table 5.2**.

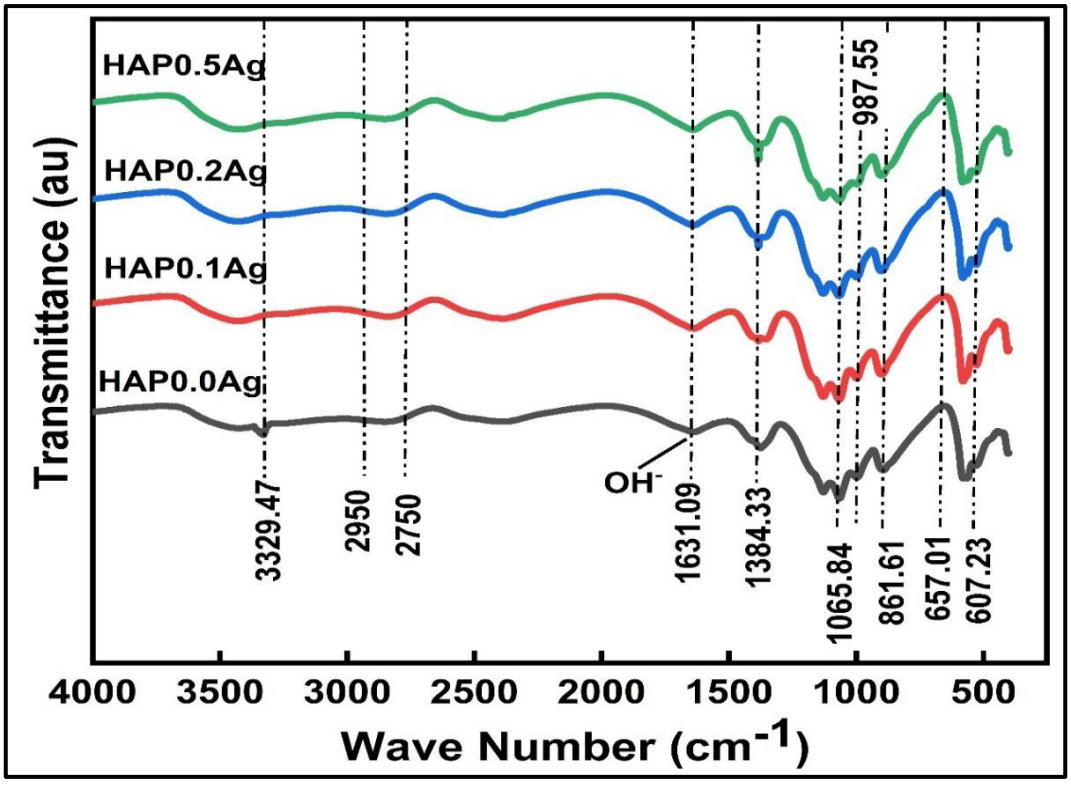

Fig. 5.8. FTIR spectra of HAP0.0Ag, HAP0.1Ag, HAP0.2Ag and HAP0.5Ag powdered samples.

Table 5.2. FTIR interpretations at different wave numbers.

Wave Number	Interpretation	Reference
607.23 cm^{-1}	O-P-O bending mode	Sebastiammal et al. [184].
657.01 cm^{-1}	O-P-O bending mode	Sebastiammal et al. [184].
1050 cm^{-1}- 850 cm^{-1}	$PO4^{3-}$ functional group and parallel P-O vibrations	Ganesan et al. [185]
1065.84 cm^{-1}, 987.55 cm^{-1} and 861.61 cm^{-1}	large intensity v_3 asymmetric stretching mode of O-P-O	Kumar et al. [186] and Chappard et al. [187]
1631.09 cm^{-1} and 3329.47 cm^{-1}	v_2 bending mode of the O-H functional group	Chappard et al. [187]
1384.33cm^{-1}	silver-based bonding	Iconaru et al. [188]
1065 - 1100 cm^{-1}	due to silver doping	Iconaru et al. [188]
Broadband 2750cm^{-1} - 2950cm^{-1}	symmetric stretching of hydrated silver-doped HAp	Kumar et al. [186],

5.1.5 X-ray diffraction Analysis

XRD spectra of eggshell-derived silver-doped hydroxyapatite from 10^0 to 80^0 2θ peak positions are characterized in **Fig. 5.9**. The crystallographic curve contains a compound whose major peaks matches with the hexagonally structured calcium hydroxyapatite having JCPDS No: 01-074-0545. As per the standard file, the crystallographic parameter has a= b= 9.4240 Å, c= 6.8790 Å, $\alpha = \beta = 90^0$ and $\gamma = 120^0$. As observed, the major planes corresponding to hydroxyapatite are (1 0 0), (1 0 1), (2 0 0), (2 0 1), (0 0 2), (1 0 2), (2 1 0), (2 1 1), (1 1 2), (3 0 0), (2 0 2), (1 3 0), (1 1 3), (2 2 2), (1 3 2), (2 1 3), (3 2 1), (1 4 0), (4 0 2), (0 0 4), (3 1 3), (3 0 4), (3 2 3) and (5 1 1) labeled at 2θ 10.83^0, 16.84^0, 21.76^0, 25.36^0, 25.89^0, 28.13^0, 28.92^0, 31.76^0, 32.19^0, 32.89^0, 34.06^0, 39.79^0, 43.88^0, 49.49^0, 50.47^0, $51,25^0$, 52.07^0, 53.28^0, 57.13^0, 63.99^0, 64.16^0 and 65^0, respectively. 2θ position 31.766^0 determines 100 % intensity of HAp compound having miller indices (2 1 1) and d- spacing 2.81468Å and the second highest peak with 60.9 % intensity is observed at 32.897^0 with miller indices (3 0 0) and d- spacing 2.72057Å. The output delivers a high level of phase purity and compound formation.

Silver doping in HAp formation has a minor impact on the compound formation and it recovers the void interplanar spaces. Some major peaks corresponding to Ag reflect substitutional effect are marked with blue club symbol in **Fig. 5.9.** at planes (1 1 1), (2 0 0) and (3 1 1). Also, the slight increase in the intensity of peaks reflects the doping characteristics of the inclusion of silver nitrate as an effective substrate for the antibacterial characterization of the modified HAP. Silver doping with 0.1 %, 0.2 % and 0.5 % molar concentration shows a little shift in 2θ value and has negligible crystallographic imperfection at higher molar concentrations. The small presence of

silver ions in HAp powder indicates that the monovalent silver ion substitutes calcium ions without the varying crystal nature of HAp [189].

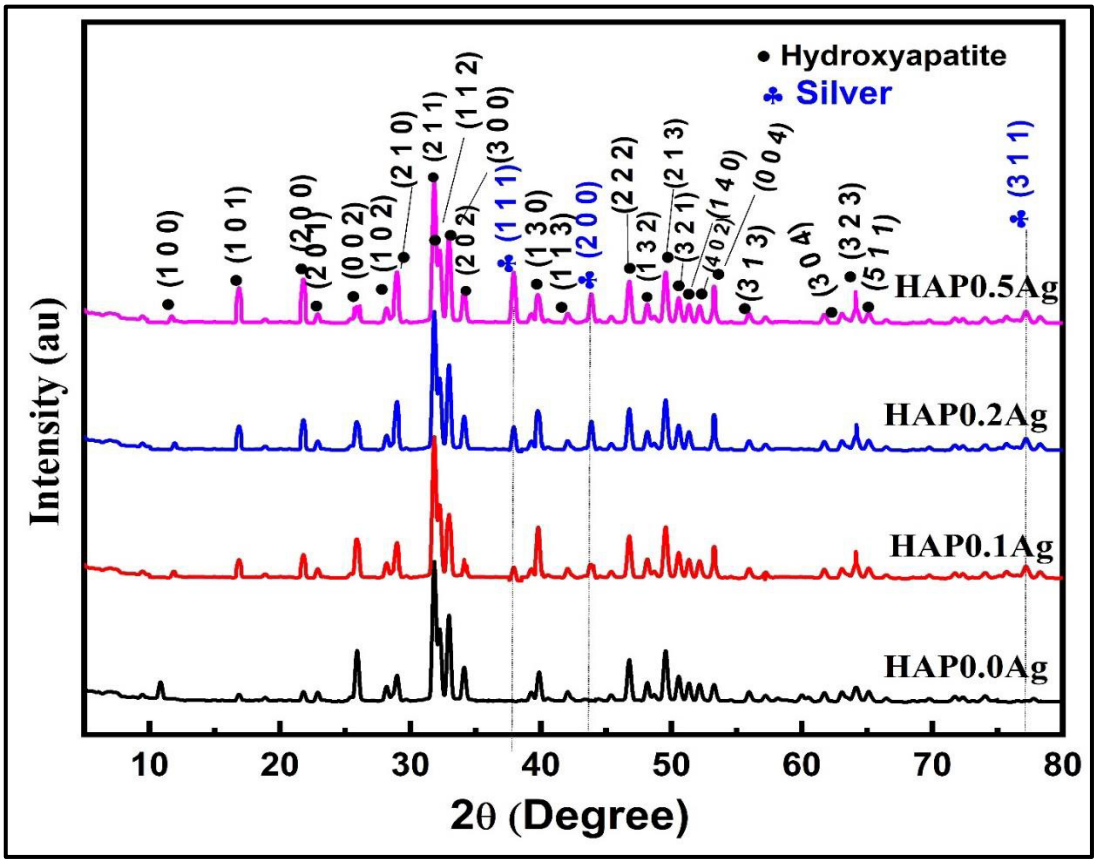

Fig. 5.9. XRD spectra of HAP0.0Ag, HAP0.1Ag, HAP0.2Ag and HAP0.5Ag powdered samples.

The higher intensity peaks are observed well between 25^0 – 40^0 2θ values. The average crystallite size with standard deviation for HAP0.0Ag, HAP0.1Ag, HAP0.2Ag and HAP0.5Ag samples obtained using Debye–Scherer's equation [190] are 505.091 ± 135.22 Å, 481.667 ± 198.21 Å, 416.417 ± 173.46 Å and 470.583 ± 141.03 Å and the average lateral strain are 0.305 ± 0.112 %, 0.303 ± 0.137 %, 0.332 ± 0.139 % and 0.301 ± 0.0814 %, respectively. Results comparison of powder diffraction characteristics are also done with the research outputs of Kostov-Kytin et al. [191] on HAp and β- TCP. The spectra validate that the silver doping at a low molar concentration in modifying

HAp provides morphological capping that can be useful for antibacterial applications without affecting its crystallographic and compositional characteristics.

5.1.6 Antibacterial Characterization

Antibacterial characterization of silver-doped HAp samples was conducted using the well diffusion method in a large-sized Petri dish.

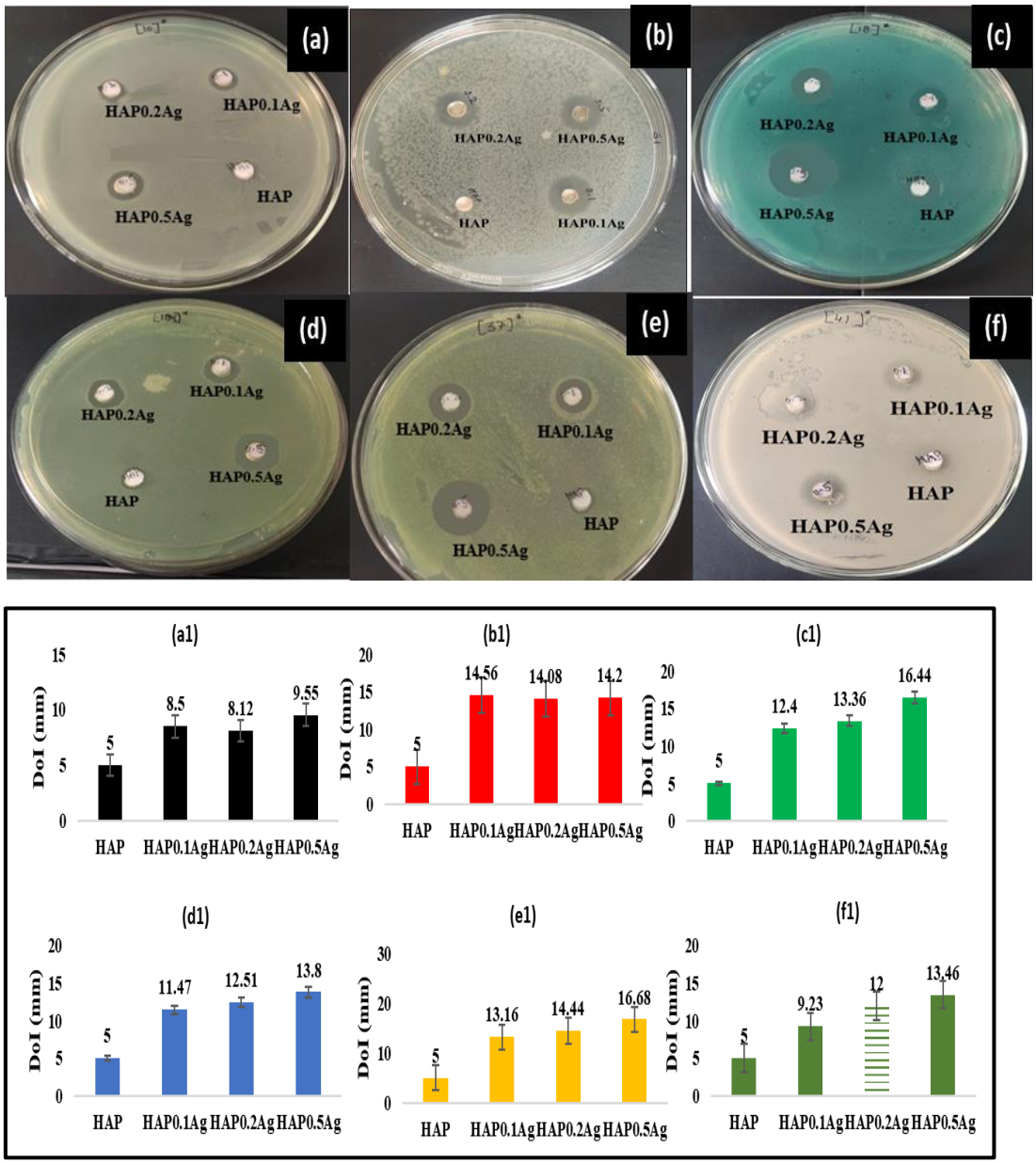

Fig. 5.10. Diameter of Inhibition for Waste Eggshell Derived Silver Doped Hydroxyapatite samples under **(a and a1)** S. Epidermidis, **(b and b1)** P. Aeruginosa **(c and c1)** E. Coli, **(d and d1)** E. Coli DH5α **(e and e1)** S. Aureus, and **(f and f1)** B. Subtilis bacterial culture after 24 hours of incubation.

The **Fig. 10 (a-f)** and **(a1-f1)** represents the pictorial view and DoI of silver-doped HAp samples, respectively obtained after 24 hours of incubation in closed environment at room temperature. As observed, silver doping enhances antibacterial characteristics compared to pure HAp (HAP0.0Ag) under all microorganisms.

The DoI with standard deviation (shown in **Table 5.3**) following multiple diametral measurements lies in the range of 5-17 mm. The maximum value of 16.68 ± 0.06 mm was observed for the HAP0.5Ag sample under the *S. Aureus* microorganism culture, which implies that the silver-doped HAp is best suited for the bacteria that cause immunity degradation. Undoped HAp does not reflect DoI greater than the well size (5 mm) and thus silver doping becomes necessary in antibacterial applications. However, a DoI less than 8mm in a 5 mm well diffusion test is considered not feasible considering the factor of safety. As observed in **Fig. 10 (f)** for HAP0.2Ag that the dissolved HAp has moved out of the well. It is because the hydroxyapatite and its derivative are insoluble in water and therefore, sometimes show agglomeration that propagates the hairline crack in the agar well during pouring [192]. Zhou et al. [193] examined the antibacterial nature of Ag-based HAp using gram-negative *E. Coli* and gram-positive *S. Aureus* microorganisms and reported that *S. Aureus* bacterial culture tests on silver nitrate-doped synthetic HAp effectively reduced the number of viable bacteria in the supernatant and on the surface of the substrate. However, *S. Epidermidis, P. Aeruginosa* and *S. Aureus* microorganisms are highly discarded and shows a high magnitude of DoI. The antibacterial activity also features the physiochemical characteristics of the silver-doped samples, such as density, particle size and conductivity of the functional group. The DoI increases with an increase in the nanoparticle of silver nitrate dopant in the HAP, but the molarity is acceptable upto a certain limit of molar concentration for effective utilization. Here, 0.5 % molar

concentration seems to be effective and maximum doping composition to attain antibacterial characterization on eggshell-derived hydroxyapatite powder. The measured DoI confirms the antibacterial nature of the synthesized samples in all the bacterial cultures and, therefore, can be a suitable substrate for biomedical coating and grafting applications.

Table 5.3. Diameter of Inhibition (Kirby- Bauer's Zone) for different Microorganism.

S. No	Code	Microorganism Name	Diameter of Inhibition (mm)			
			HAP0.0Ag	HAP0.1Ag	HAP0.2Ag	HAP0.5Ag
1	{10}	S. epidermidis	05.00 ± 00	08.50 ± 0.21	08.12 ± 0.10	09.55 ± 0.18
2	{12}	P. Aeruginosa	05.00 ± 00	14.56 ± 0.10	14.08 ± 0.16	14.20 ± 0.06
3	{18}	E. Coli	05.00 ± 00	12.40 ± 0.56	13.36 ± 0.25	16.44 ± 0.1
4	{18α}	E. Coli DH5α	05.00 ± 00	11.47 ± 0.20	12.51 ± 0.11	13.80 ± 0.11
5	{37}	S. Aureus	05.00 ± 00	13.16 ± 0.31	14.44 ± 0.32	16.68 ± 0.21
6	{41}	B. Subtilis	05.00 ± 00	09.23 ± 0.23	12.00 ± 0.10	13.46 ± 0.17

5.1.7 Wettability Analysis

Water absorption tests on the synthesized samples were performed for six days. The percentage of water absorbed with time is plotted as shown in **Fig. 5.11.** The initial dried sample of HAP0.0Ag, HAP0.1Ag, HAP0.2Ag and HAP0.5Ag weighed 1.56 g, 1.82 g, 1.61 g and 2.11 g, respectively, and it was increased by 1.49 %, 1.32 %, 1.25 % and 1.16 % after eight hours of immersion. The sample weights were taken continuously until the constant mass between three consecutive readings was observed. The maximum water absorption was observed in undoped HAp (HAP0.0Ag, 1.974 %) after 144 hours. As observed, the Ag doping improves the water- soaking ability of the samples, and thus the reduction in open pores is interpreted.

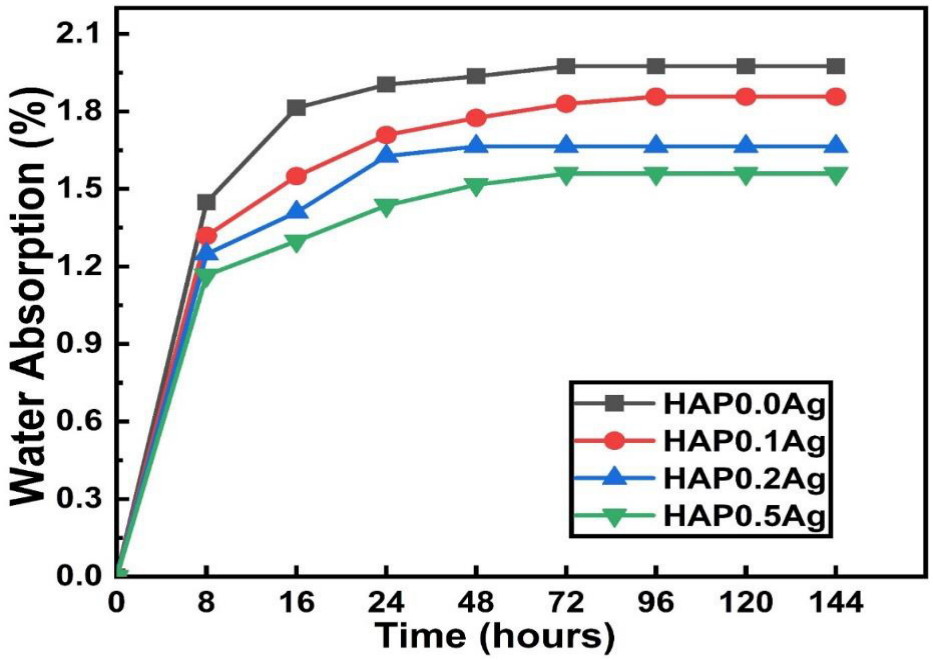

Fig. 5.11. Water Absorption (%) of silver-doped hydroxyapatite composite with time (hours).

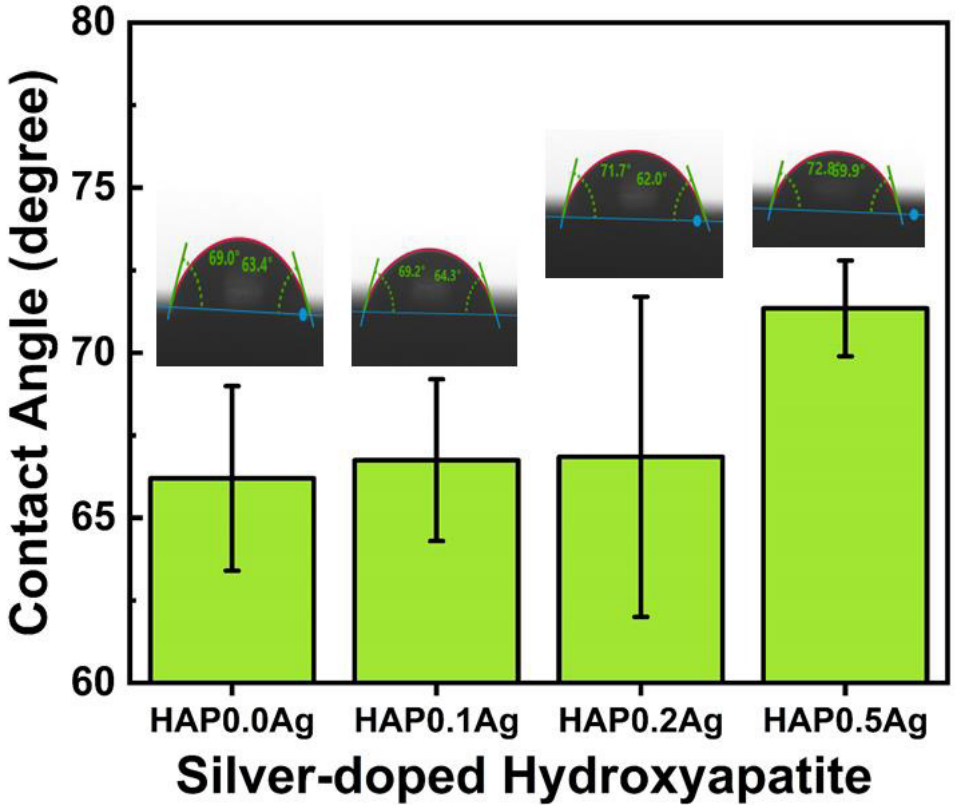

Fig. 5.12. Contact angle of silver doped hydroxyapatite.

The percentage of water absorption also decreases with an increase in Ag doping concentration in HAp and divulges the slight hydrophobicity of doped samples, which

is also testified during contact angle measurement. Reis et al. reported increased flexural strength of an acrylic-based denture resin after 30 days of immersion [194]. The flexural change could be due to the continuous polymerization of the monomer, which acts as a plasticizer and leaches from the specimen to increase flexural strength. The specimen's weight variation was a combination of weight rise due to absorption and weight loss caused by sample leaching [195]. The wettability of the silver-doped hydroxyapatite samples examined using contact angle is shown in **Fig. 5.12.** The average ± SD value of the contact angle for HAP0.0Ag, HAP0.1Ag, HAP0.2Ag and HAP0.5Ag are 66.2 ± 2.8, 66.75 ± 2.45, 66.85 ± 4.85 and 71.35 ± 1.45, respectively. The values thus obtained show the hydrophilic nature of the HAPAg samples. The low contact angle for HAp promotes higher surface courage in coating applications [162]. The hydrophilic material exhibits better results in biomedical applications, diagnostic devices, drug delivery, surface coating, heat dissipation and hydrogel applications. Maidaniuc et al. [161] reported that the contact angle of HAp was influenced by particle size and forming pressure.

The calculated and the direct magnitude of SFE for the silver-doped hydroxyapatite samples are graphed in **Fig. 5.13 .** SFE contributes to cell adhesion to HAp through wettability [196]. It is the inverse of the contact angle and influences an implant's biological interactions [197]. The calculated values are obtained using Owens Wendt Equation [198], while the direct values were obtained from the CA measurement machine through distilled water and diazomethane droplets. The decrease in the mean values of total SFE with the increase in doping concentration reveals the hydrophobicity of the silver-doped samples, which directly correlates with the water absorption % and the contact angle. The E_s^d and E_s^p values for HAP0.0Ag was 29.43 mJ/m^2 and 13.62 $mJ/m^{2,}$ whereas HAP0.5Ag decreased to 26.28 mJ/m^2 and 11.92

mJ/m^2, respectively. The mean ± SD of the contact angle and SFE are tabulated in **Table 5.4.** SFE determines the wettability and adhesion characteristics of the liquid with solid surfaces [199]. Szcześ et al. [200] compared the SFE between synthetic and natural (obtained from pig bones) HAp using the thin-layer wicking method and concluded that the average total SFE for natural HAp is slightly higher than synthetic HAp. However, the result obtained in the current research has a total SFE lower than that reported by Szcześ et al. [200]. The variation in the precursor, the methodology adopted, and doping concentration directly affect total SFE magnitude.

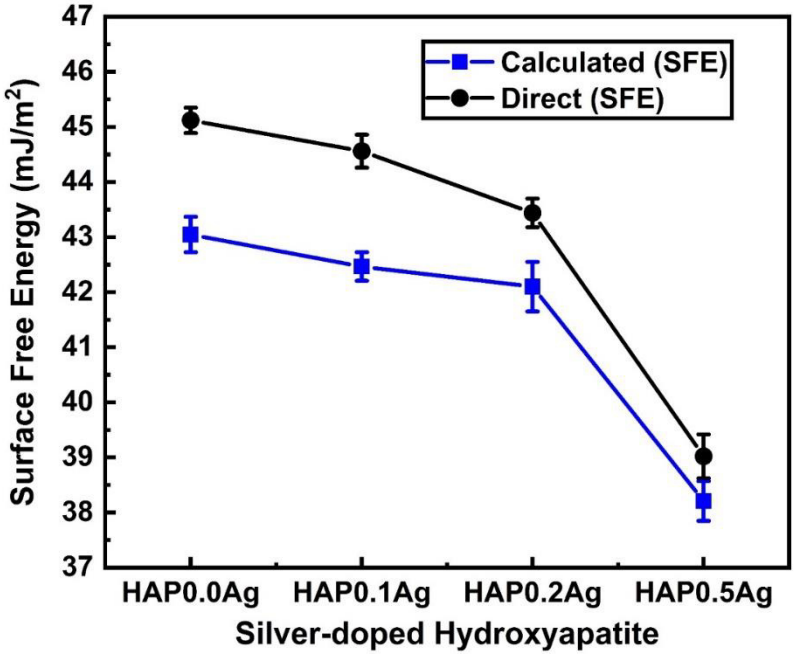

Fig. 5.13. Surface free energy of the silver-doped HAp**.**

Table 5.4. Contact angle and surface free energy values for silver-doped HAp samples.

Sample	Contact Angle		Total Surface Free Energy		Error %
	water droplet	Diiodomethane Droplet	Calculated	Instrumental	
HAP0.0Ag	66.20 ± 2.80	58.40 ± 1.41	43.05 ± 0.32	45.12 ± 0.23	4.81
HAP0.1Ag	66.75 ± 2.45	59.17 ± 1.82	42.47 ± 0.26	44.56 ± 0.30	4.92
HAP0.2Ag	66.85 ± 4.85	60.12 ± 3.12	42.10 ± 0.45	43.44 ± 0.26	3.18
HAP0.5Ag	71.35 ± 1.45	63.89 ± 2.12	38.21 ± 0.36	39.02 ± 0.40	2.12

5.1.8 Thermal Analysis

TGA results of the powdered samples are illustrated in **Fig. 5.14 (a)**. The curve represents the percentage of weight loss with the increased temperature of the synthesized powder. As observed, the mass decomposition was between 6.9- 8.4% till 1000^0C, depending upon the doping concentration of the powdered sample. The initial weight loss between 23-250^0C is attributed to the absorbed water during chemical synthesis [201]. The degradation in the mass near 250^0C- 450^0 corresponds to the conversion of hydrogen phosphate (HPO_4^{2-}) to phosphate (PO_4^{3-}) via pyrophosphate ($P_2O_7^{4-}$), releasing water of hydration as shown in equations (5.1 and 5.2).

$$2HPO_4^{2-} \rightarrow P_2O_7^{4-} + H_2O \uparrow \quad ...(5.1)$$

$$P_2O_7^{4-} + 2OH^- \rightarrow 2PO_4^{3-} + H_2O \uparrow \quad ... (5.2)$$

The minimum mass loss (6.935%) was observed in HAP0.1Ag and the maximum (8.388%) in HAP0.5Ag. The mass loss rate in HAP0.0Ag is minimum till 350^0C. However, the total mass loss in HAP0.0Ag was observed to be 7.4776% which is 0.54% more than the HAP0.1Ag, which can be due to the decomposition of the phosphate phase in undoped HAp or the interstitial water loss reported by Lazic et al. [202]. Also, silver doping may act as a binding agent when treated at higher temperatures. Mass loss in HAP0.2Ag retains 92.29% of the total mass till 1000^0C.

The degradation rate is minimal in undoped HAp and shows increasing trends with an increase in silver doping. HAP0.5Ag has a maximum mass loss, and the loss is at a comparatively lower temperature than other sequential compositions. It may be due to the release of nitrate ions, as nitrates are easily replaceable. It is interesting to note that the HAP0.0Ag and HAP0.1Ag curves cross at 456.23^0C. The remaining weight of sample HAP0.0Ag and HAP0.1Ag at an instant is the same, i.e., 93.155%. It is the instantaneous temperature where both compositions have the same degradation rate.

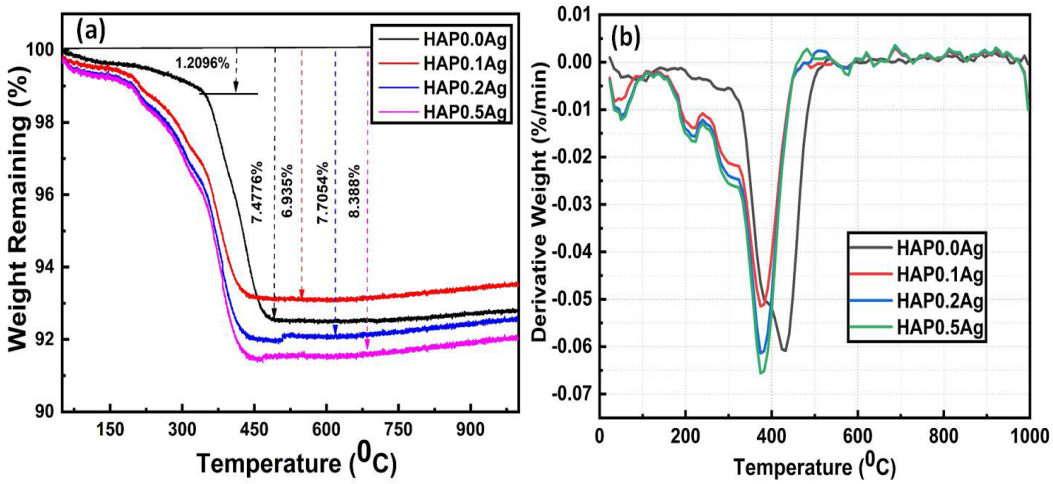

Fig. 5.14. (a) Thermal Gravimetric Analysis (TGA) and **(b)** Derivative Thermogravimetric (DTG) Curve of eggshell-derived silver-doped HAp.

It implies that HAp with 0.1 wt% of silver doping can also be the optimum composition for thermally stable silver-doped HAp. A similar observation was seen in **Fig. 5.1 (d),** where the porosity and relative density curve meets between zero and 0.1% doping. The DTG curve in **Fig. 5.14 (b)** shows the decomposition in phase near 400 ^{0}C where the weight derivative measured in weight remaining percent per min is minimum magnitude between 350-450 ^{0}C. The curve helps to determine the temperature associated with the phase transformation [203]. The rate of mass decomposition depends upon the percentage of doping in the HAp. It is probably because the increase in temperature first decomposes the impurity present in the stable calcium hydroxyapatite, which is highest in HAP0.5Ag. The negligible mass loss between 500 ^{0}C and 1000 ^{0}C concludes and confirms the high thermal stability of HAp at higher temperatures.